J Mater Sci: Mater Med (2010) 21:753–760
DOI 10.1007/s10856-009-3872-4

Fabrication and biocompatibility of nano non-stoichiometric apatite and poly(ε-caprolactone) composite scaffold by using prototyping controlled process

Liang Ye · Xinchen Zeng · Haojiang Li · Yi Ai

Received: 30 June 2009 / Accepted: 9 September 2009 / Published online: 27 September 2009

Abstract Nano biocomposite scaffolds of non-stoichiometric apatite (ns-AP) and poly(ε-caprolactone) (PCL) were prepared by a prototyping controlled process (PCP). The results show that the composite scaffolds with 40 wt% ns-AP contained open and well interconnected pores with a size of 400–500 μm, and exhibited a maximum porosity of 76%. The ns-AP particles were not completely embedded in PCL matrix while exposed on the composite surface, which might be useful for cell attachment and growth. Proliferation of MG_{63} cells was significantly better on the composite scaffolds with porosity of 76% than that those with porosity of 53%, indicating that the scaffolds with high porosity facilitated cell growth, and could promote cell proliferation. The composite scaffolds were implanted into rabbit thighbone defects to investigate the in vivo biocompatibility and osteogenesis. Radiological and histological examination confirmed that the new bony tissue had grown easily into the entire composite scaffold. The results suggest that the well-interconnected pores in the scaffolds might encourage cell proliferation, and migration to stimulate cell functions, thus enhancing bone formation in the scaffolds. This study shows that bioactive and biocompatible ns-AP/PCL composite scaffolds have potential applications in bone tissue engineering.

L. Ye
Guanghua School of Stomatology, Sun Yat-sen University, 510080 Guangzhou, People's Republic of China
e-mail: liangye456@yahoo.cn

X. Zeng (✉) · H. Li (✉)
Zhongshan School of Medicine, Sun Yat-sen University, 510080 Guangzhou, People's Republic of China
e-mail: xinchenbio@yahoo.cn

H. Li
e-mail: haojiangmaterial@yahoo.cn

Y. Ai
College of Life Sciences, Sun Yat-sen University, 510080 Guangzhou, People's Republic of China

1 Introduction

Many studies have shown that nano hydroxyapatite (n-HA) biomaterial had excellent bioperformance and was a potential candidate for hard tissue repair [1–4]. Nevertheless, the extensive use of n-HA is still limited by its powder state and brittle nature. Biodegradable polymers and their copolymers are widely used in bone regeneration, dental repair, orthopedic fixation devices, as well as many other biomedical applications [5, 6]. However, there exist no pure polymers that can effectively bond to bone in vivo, and organic/inorganic biocomposites of degradable polymers and bioactive inorganic phases are still a promising approach to develop bioactive biomaterials for bone repair [7, 8]. Poly(ε-caprolactone) (PCL), one of the most commercially available biodegradable polymers, is widely used in biomedical fields for its biodegradability, biocompatibility, and formability [9, 10].

Studies suggested that the variation in the molar ratio of calcium to phosphate greatly affected the solubility of the Ca–P biomaterials, and apatite with Ca/P of 1.50 degraded faster than hydroxyapatite with Ca/P of 1.67 when implanted in vivo [11, 12]. Previous studies showed that calcium deficient apatite (also called non-stoichiometric apatite, ns-AP) with Ca/P of 1.50 was biologically more active than pure HA because it has a composition and structure very close to natural bone mineral, and therefore has been considered to be the ideal material for bone repair

[13]. Therefore, it is expected that fabrication of nano non-stoichiometric apatite (ns-AP) for novel bone regeneration material will improve the bioperformance of apatite biomaterial. A combination of PCL with bioactive ns-AP is likely to bring the advantages of both biomaterials.

Several methods have been proposed for fabrication of porous scaffolds, including particulate leaching, gas foaming, electrospinning, freeze drying, foaming of ceramic from slurry, and the formation of polymeric sponge [14–16]. However, scaffolds preparation using these methods have some shortcomings in controlling the structure and interconnectivity of pores, which may limit their application in terms of cell penetration in tissue engineering. To obtain scaffolds with high porosity and good interconnectivity, new techniques need to be developed. Recently, some researchers proposed the techniques for fabricating three-dimensional (3D) scaffolds with controllable porosity and well-defined 3D microstructures using rapid prototyping (RP) methods, such as fused deposition modeling, selective laser sintering, 3D printing^{TM}, multiphase jet solidification, and 3D plotting [17–20]. In this study, ns-AP/PCL composite scaffolds were prepared using a prototyping controlled process, and the cell/tissue responses to the composite scaffolds both in vitro and in vivo were investigated.

2 Materials and methods

2.1 Synthesis of ns-AP

The ns-AP was synthesized using calcium nitrate ($Ca(NO_3)_2{\cdot}4H_2O$) and ammonium phosphate ($(NH_4)_2HPO_4$). First, calcium nitrate and ammonium phosphate (Ca/P mol ratio = 1.50, calcium nitrate/ammonium phosphate) were dissolved separately in deionized water. The ammonium phosphate solution was dropped slowly into the calcium nitrate solution while stirring at room temperature. The pH of the solution was kept between 10 and 12 by adding ammonium hydroxide. After the titration was completed, the mixture was set at room temperature for 24 h. The resulting apatite precipitate was washed with deionized water for five times, placed in a flask, and treated in deionized water for 2 h at 100°C. After treatment, the apatite precipitate (ns-AP) was in slurry state. The ns-AP slurry and dimethyl formamide (DMF) were mixed in a beaker while stirring, and the temperature was gradually increased to 120°C. After all the water had evaporated, a mixture of ns-AP/DMF slurry was obtained. An aliquot was removed for transmission electron microscopy (FE-TEM, JEM-2100F, JEOL, Tokyo, Japan) testing. The surface morphology of the ns-AP dried powders was examined by scanning electron microscopy (FE-SEM, S-4300SE, Hitachi Ltd, Tokyo, Japan), all the chemicals used were purchased from Sinopham Chemical Reagent Co., Ltd.

2.2 Fabrication of ns-AP/PCL scaffolds

The 3-D robotic system used to fabricate ns-AP/PCL scaffolds was composed of three components: the pressure pump was used to control extrusion rate of composite slurry, whereas the robotic system and computer were used to control the morphology of the composite scaffolds and the speed of scanning. The composite slurry was extruded into the plotting medium (ethanol solution) from the syringe and many scans were used to make a scaffold. Briefly, PCL pellets (MW = 60,000: Sigma–Aldrich Co, St. Louis, MO, USA) were dissolved in chloroform at a concentration of 10% (w/v) and enough ns-AP/DFM slurry was added to produce composites with 40 wt % ns-AP content. The mixture was stirred continuously for 4 h to obtain composite slurries, which were then placed into a syringe-like injector. The composite slurry was extruded into the plotting medium to obtain a porous construct. Composite scaffolds were fabricated by extruding the slurry at a controlled extrusion rate of 50 μl/min and a scan speed of 8 mm/s. To eliminate the solvent completely, the scaffolds were immersed in distilled water for over 2 days and then freeze-dried for over 3 days. The fabricated scaffolds were stored in a desiccator until use.

2.3 Characterization of composite scaffolds

The surface phase composition of the ns-AP/PCL composite was examined by X-ray diffraction (XRD, Geigerflex, Rigaku Co., Japan). The surface morphology of the composite scaffolds was examined by scanning electron microscopy (SEM) and atomic force microscopy (AFM), and the porosity of the scaffolds was measured in distilled water by the Archimedes method. The average porosity was calculated based on five samples. The mechanical strength of the composite scaffold samples ($10 \times 10 \times 10$ mm^3) was measured (the samples were compressed in perpendicular to the 'planes' of the extruded fibers until failure) at room temperature using a compression test at a constant displacement rate of 2 mm/min. The jigs were specially designed to provide a uniform load on the composite samples, and a Bionix 858.20 (MTS Systems Corp. Eden Prairie, MN, USA) was used to conduct tests. The surface area was measured to convert the compressive loads into compressive stresses. The compressive modulus was determined from the initial linear region. Five samples were tested for each group, and the average and standard deviation were calculated for statistical analysis.

2.4 Cell proliferation

Samples ($10 \times 10 \times 5$ mm^3) of the composite scaffolds with porosities of 76 and 53% were sterilized by using ultraviolet light for 30 min. The proliferation of MG_{63} cells cultured on the samples was assessed quantitatively using MTT assay (tissue culture plate as a control). Samples were first put in each well of the 96-well plate. MG_{63} cells were then seeded onto the samples at a density of 3×10^4 cells/sample, followed by incubation at 37°C and 100% humidity with 5% CO_2 in a DMEM-BFS medium. The medium was changed every 2 days. After culturing for 1, 3 and 5 days, 100 μl methyl thiazolyl tetrazolium (MTT) solution was added into each well in the plate. The plate was then incubated for a further 4 h. The supernatant of each well was then removed and 200 μl dimethyl sulfoxide (DMSO) added. After shaking for 10 min, the optical density (OD) at 490 nm was measured with an enzyme-linked immunoadsorbent assay plate reader. Six samples of each kind were tested after each culture time, and each test was performed in triplicate.

2.5 Biocompatibility and osteogenesis in vivo

Biocompatibility and osteogenesis in vivo of the composite scaffolds were evaluated using macroscopic and histological methods. Briefly, the healthy New Zealand white rabbits weighing about 3.0 kg each were used for the implantation of the composite scaffolds. The rabbits were anesthetized with pentobarbital sodium. A critical-sized defect, measuring about $10 \times 10 \times 10$ mm^3, was made in the tibia of each rabbit. A scaffold of about the same size was inserted into the defect and fixed with a titanium plate. The rabbits were sacrificed at 4 and 8 weeks after the operation. Sacrificed tibias were examined radiologically after sacrifice. Constructs of sacrificed scaffold were imaged using a high resolution micro-computed tomography system (μ-CT 40, Scanco Medical, Bassersdorf, Switzerland). The scanner was set to a voltage of 55 kV, at a current of 145 mA so as to allow sufficient energy. Samples were scanned at 8 m voxel (3D pixel) resolution with an integration time of 120 ms to produce 3D reconstructed images. The scaffolds together with surrounding tissue were excised, fixed in 10% neutral buffered formalin, decalcified and embedded in paraffin. Tissue blocks were sectioned to 4 μm in thickness and stained with H&E, and observed with light microscope (CX21, Olympus, Japan).

2.6 Statistical analysis

Statistical analysis was performed using one-way ANOVA with post hoc tests. All results are expressed as the mean ± standard deviation (SD). Differences were considered statistically significant at $P < 0.05$.

3 Results

3.1 Characterization of scaffolds

Figure 1a shows the SEM micrograph of the morphology of ns-AP. It is found that the ns-AP present ball-like particles with the size of around 50 nm (ns-AP powders agglomeration). Figure 1b shows a transmission electron micrograph of the ns-AP morphology. It is observed that the ns-AP is rod-shaped grains with the size of 20–40 nm in diameter and 70–90 nm in length.

Figure 2a presents the fabrication of ns-AP/PCL composite scaffold by prototyping controlled process. Photograph of the 3D ns-AP/PCL composite scaffolds indicate that the scaffold had well-interconnected, uniformly distributed pores (Fig. 2b). The porosity of the prepared composite scaffolds in this study ranged from 53 to 76%. The compressive strength of the composite scaffolds decreased with increasing porosity as shown in Table 1. It can be seen that the compressive strength of the composite scaffold varied from 2.7 to 6.9 MPa as the porosity varied from 76 to 53%.

Figure 3 shows the surface morphology and microstructure of the ns-AP/PCL composite scaffolds. The composite scaffold exhibits a macroporous structure with completely open and interconnected pores. The pore size of the scaffolds ranged from 400 to 500 μm in both the vertical direction and horizontal directions, with interconnected pores in three dimensions.

Examination at greater magnifications by SEM (Fig. 4a) reveals that the composite scaffold surface exhibited typical spherical granules of apatite with the particles size of around 100 nm (some ns-AP particles congregation). It can be seen that most apatites (arrow) were exposed on the composite surface except some ns-AP granules were embedded in PCL matrix. The atomic force microscopy (AFM) photograph of ns-AP/PCL composite is shown in Fig. 4b. It is found that the ns-AP particles with the sizes of around 50 nm were homogeneously distributed in PCL matrix and combined with PCL in the composite.

The XRD pattern of the composite surface analysis is shown in Fig. 5. The results show that there are peaks at $2\theta = 25.9°$, 28.4°, 32.4°, 33.2°, 39.7°, and 48.3°, which are characteristic peaks of apatite. It can be concluded that ns-AP particles are exposed on the composite surface, and are not completely embedded in PCL matrix. Moreover, it is found that the composite consists of ns-AP and PCL phase, and the ns-AP presents apatite phase with low crystallinity, no additional phase was identified within detectable limits.

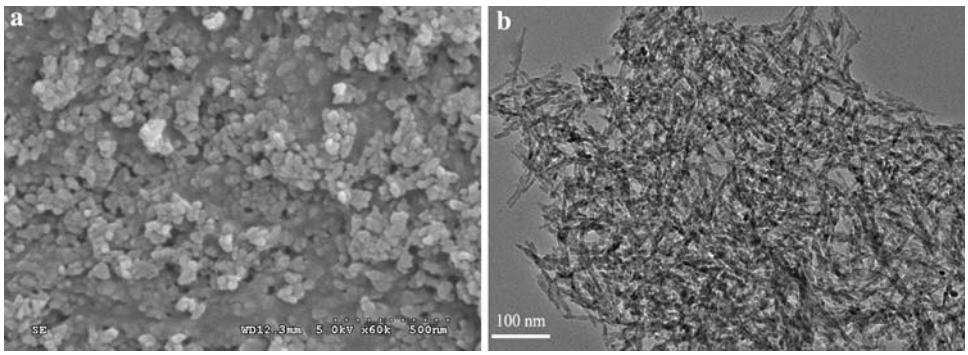

Fig. 1 **a** SEM and **b** TEM micrographs of ns-AP

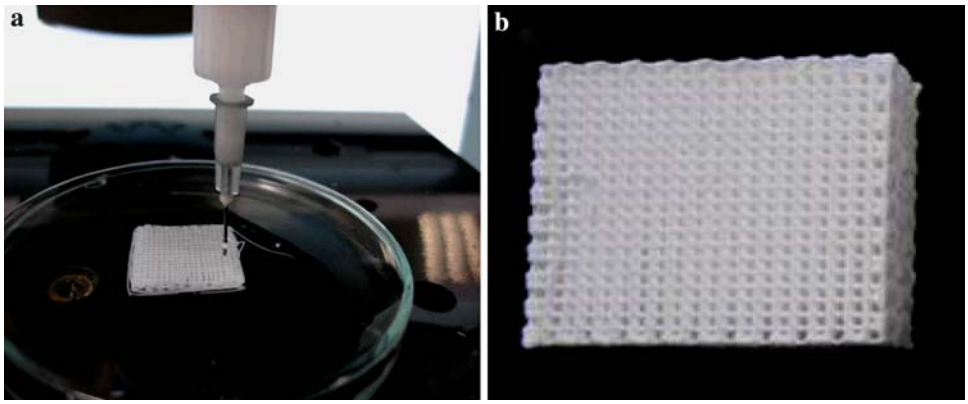

Fig. 2 **a** photograph of prototyping controlled process for fabrication of composite scaffold, and **b** composite scaffold

Table 1 Effects of porosity on compressive strength and compressive modulus of composite scaffolds with 40 wt% ns-AP

Specimens	Porosity (%)	Compressive strength (MPa)	Compressive modulus (MPa)
1	76 ± 4	2.7 ± 0.8	1.5 ± 0.2
2	65 ± 2	4.6 ± 1.0	2.8 ± 0.5
3	53 ± 3	7.9 ± 1.2	3.4 ± 0.5

3.2 Biocompatibility and osteogenesis

Proliferation of MG_{63} osteoblast-like cells cultured on composite scaffolds with porosities of 76 and 53% was assessed using the MTT assay because OD values can provide an indication of cell growth and proliferation on various biomaterials. Figure 6 reveals that OD values for the composite with porosity of 76% were significantly higher than 53% and control at 3 and 5 days ($P < 0.05$); no significant differences appeared after 1 day. These results indicate that cell growth and proliferation (at 3 and 5 days) was superior in the composite with porosity of 76% than those for the composite with 53% porosity and the control, suggesting that composite with high porosity facilitates cell growth and can promote cell proliferation.

Micro-CT was used to examine the bony tissue formed into the composite scaffold. Figure 7 presents micro-CT images after 8 weeks. In general, bone tissue responses to the scaffolds were excellent, as the bone grew well into the whole scaffold. After 8 weeks of implantation, scaffolds are shown in both sagittal [(a), (b), (c)] and transverse directions [(d), (e), (f)]. These images confirm deep ingrowth of osteoid into the scaffolds, and show direct attachment of new bone tissue to the surfaces of the scaffolds. The sagittal and transverse of micro-CT images show that dense bone tissue had formed gradually in the scaffolds.

Histological analysis of H&E stained sections reveal that new bone formation into the scaffolds, as shown in Fig. 8. After implantation for 4 weeks, the new osteoid matrix formation inside the scaffolds was observed (Fig. 8a). The osteoid matrix was well distributed throughout the scaffolds with some mineralization, and a large number of osteoblasts were observed around the newly formed osteoid matrix. There was no severe inflammation or adverse tissue reaction associated with any of the implanted composite scaffolds.

At 8 weeks after implantation, much new bone had formed between the original bone and the scaffolds, and

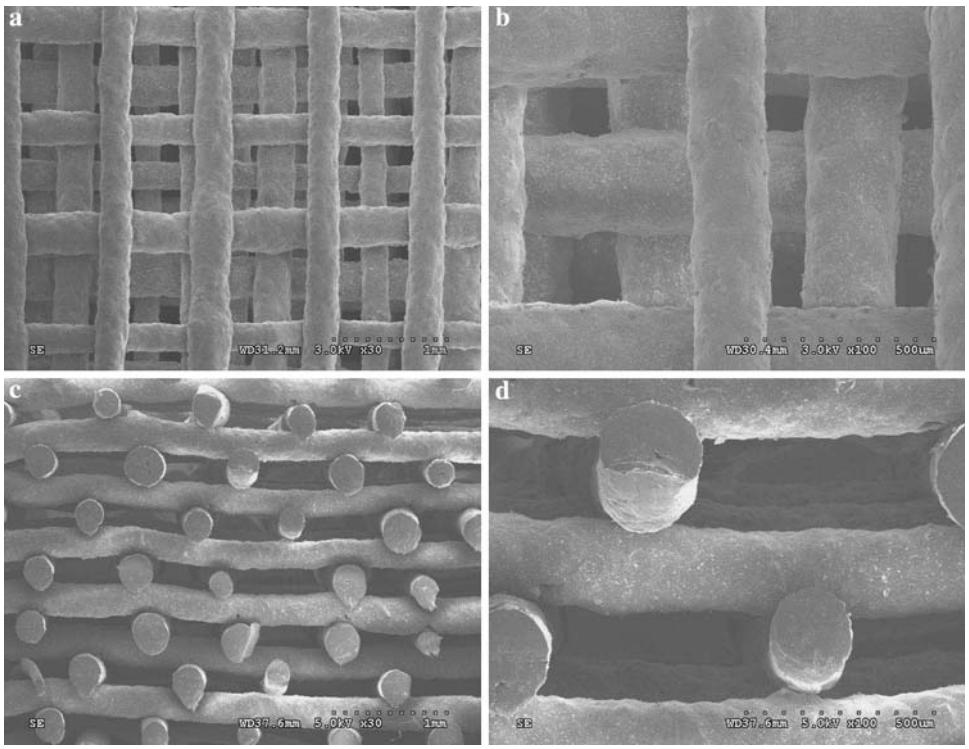

Fig. 3 SEM micrographs of the ns-AP/PCL composite scaffolds, sagittal (a—×30, b—×100), transverse direction (c—×30, d—×100)

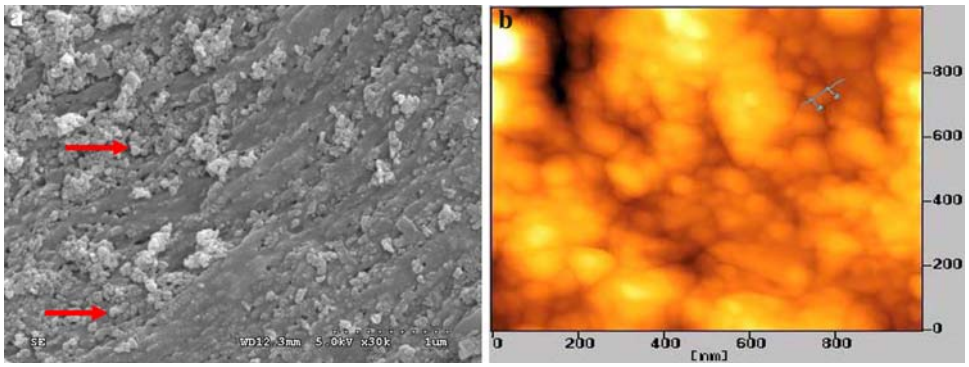

Fig. 4 SEM (**a**) and AFM (**b**) micrographs of the surface morphologies of composite scaffolds

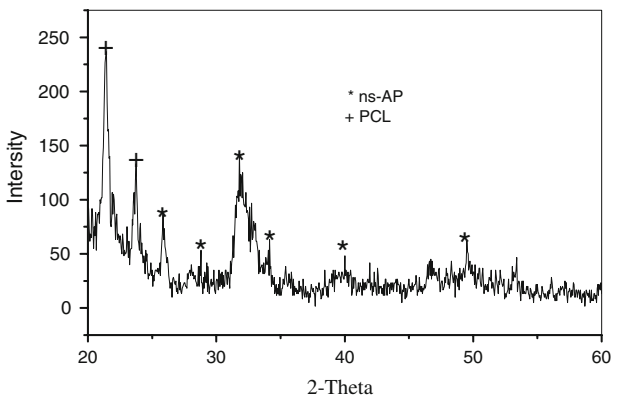

Fig. 5 XRD patterns of the surface of the ns-AP/PCL composite scaffold

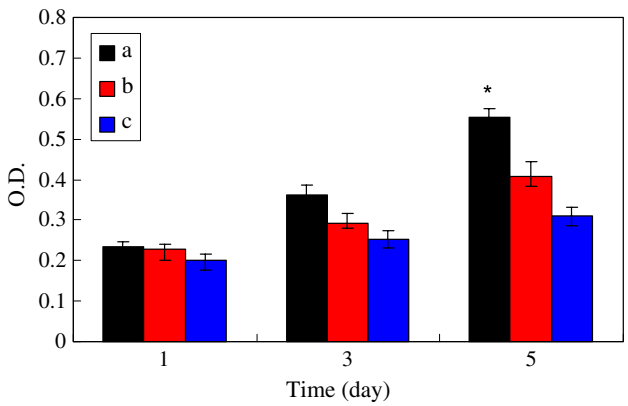

Fig. 6 Proliferation of osteoblast on the composite scaffolds with porosity of **a** 76%, **b** 53% over time ($n = 5$, $^*P < 0.05$), **c** control

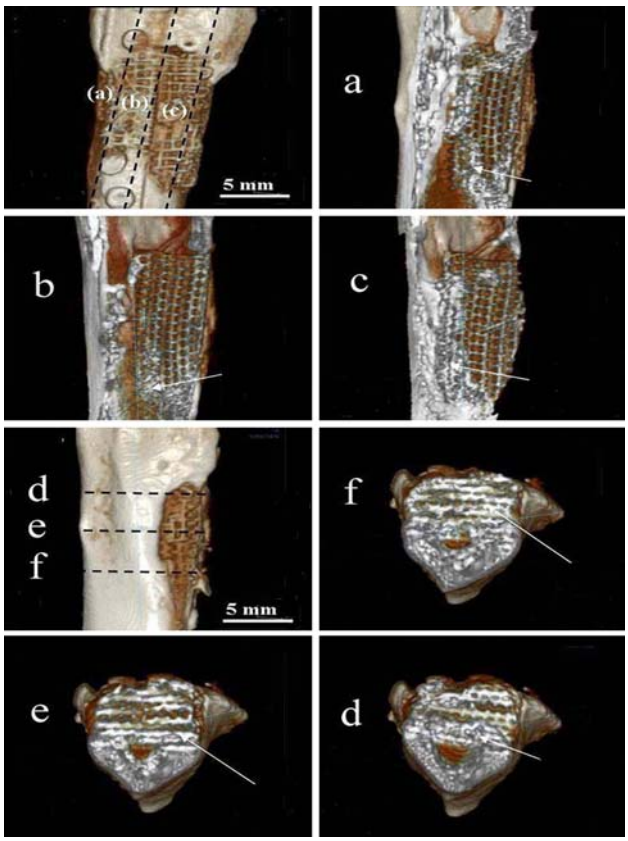

Fig. 7 Micro-CT images after 8 weeks implantation. Images of the composite scaffolds were divided into three equal parts to sagittal (**a**–**c**) and transverse direction (**d**–**f**)

many osteocytes and osteoblasts were present in the newly formed bone. Some new bone tissue even interconnected to form circles around the scaffolds, indicating a good interface between the new bone and the implanted scaffolds. Some sporadic fatty marrow cells were also observed around the scaffold.

4 Discussions

A biocompatible porous scaffold is important as a temporary carrier for implanted cells in bone tissue engineering, and the scaffolds should have high levels of porosity, suitable pore size, and highly interconnected pore structure [21]. Cell growth and new tissue formation are dependent on the porosity, pore size, and material of the scaffolds. An interconnecting pore network is also essential for tissue ingrowth, vascularization, and nutrient diffusion [14]. It was found that pores between 50 and 150 μm determine osteoid growth, and pores larger than 150 μm facilitate cell proliferation, vascular ingrowth, and internal mineralized bone formation [22]. It is difficult to control the pore size and morphology, and maintain interconnected pores using conventional methods such as particulate leaching [15, 23].

In this study, ns-AP/PCL bioactive composite porous scaffolds were fabricated by using a prototyping controlled process (PCP), in which the pore size and porosity of the scaffolds could be controlled by computer system. The scaffolds exhibited a homogeneous distribution of open macropores and pore sizes mainly in the range of 400–500 μm. Moreover, this study revealed that the composite scaffold contained well interconnected pores. Therefore, the characteristic of the composite scaffolds is likely to be beneficial in facilitating cell infiltration and bone ingrowth. The porosity of the composite scaffold had an obvious effect on the compressive strength. The higher the porosity, the lower the compressive strength of the scaffold, and the scaffolds with the greatest porosity of 76%, had the lowest compressive strength and compressive modulus of 2.7 and 1.5 MPa, respectively. Samples with a porosity of 53% had compressive strength and compressive modulus values of 7.9 and 3.4 MPa, respectively.

For apatite/polymer bioactive composites, interface and surface properties of the composite are very important. The

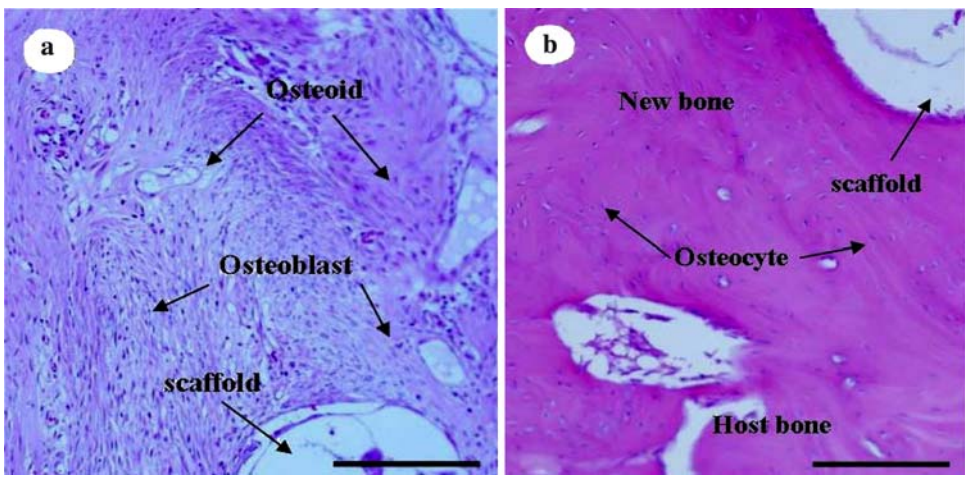

Fig. 8 Histological appearances of rabbit thighbone defect implanted with ns-AP/PCL composite scaffolds for **a** 4 weeks and **b** 8 weeks. (H&E, ×100), *bar* = 200 μm

bioactivity and other performances of the nano apatite/polymer composite are related to the dispersion of apatite in the composite [24]. When the apatite distributes uniformly in the polymer and is exposed on the surface of the composite, the composite has good bioactivity and surface properties, and easily forms bone-binding with natural bone [25]. However, if apatite is embedded in the polymer, it will have low bioactivity. In the present study, the results indicate that the apatite particles were not completely embedded in the polymer PCL but were exposed on the composite surface, which can provide bioactivity for the composite when is used as implant.

Ideally, bioactive biomaterials need to interact actively with cells and stimulate cell growth [26]. It was observed in this study that the MG_{63} cells were able to proliferate on the composite scaffolds, as demonstrated by the MTT assay. Our results reveal that the composite scaffolds with porosities of 76 and 53% could both stimulate the growth and proliferation of MG_{63} osteoblast-like cells over time, and the cell proliferation on the composite scaffolds significantly depended on the porosity of the scaffolds. The higher the porosity, the greater the cell proliferation on the scaffolds. In addition, the enhancement of the proliferation of MG_{63} cells on the composite scaffold is likely to be associated with the surface features of the composite scaffold. The composite surface features (nano-sized apatite exposed on the composite surface) might be responsible for stimulating cell growth and proliferation because of its small size and bioactivity. Webster and co-workers [27, 28] observed a significant increase in protein adsorption and osteoblast adhesion on nanosized ceramic materials compared with the traditional microsized ceramic materials, and the mutual effect with the formation of extracellular matrix was even more significant.

The results of in vitro experiments prompted us to investigate the bioproperties of the composite scaffold in vivo. In general, if the bone tissue responses to the scaffolds are excellent, the bone tissues would grow well into the implanted scaffolds. In this study, Micro-CT was used to examine the new bone tissue formed into the composite scaffold after 8 weeks. The results confirm that the osteoid had grown into whole scaffolds, and the new osteoid was quite extensive, with direct attachment to the surfaces of the scaffold, and appeared to penetrate deeply into the scaffold. Furthermore, the micro-CT images showed that dense bone tissue had formed gradually in the composite scaffold.

Histological analysis revealed that the new osteoid matrix had formed inside the composite scaffold after implantation for 4 weeks. The osteoid matrix was well distributed throughout the scaffolds with some mineralization, and a large number of osteoblasts were present around the newly formed osteoid matrix. Much new bone was formed between the original bone and the scaffold at 8 weeks, and many osteocytes and osteoblasts were found in the new bone. These results indicate that the incorporation of ns-AP into the porous composite scaffold, with its well interconnected pores, had a positive effect on encouraging the formation of bone. In summary, the ns-AP/PCL composite scaffolds presented not only good biocompatibility but also faster and more effective osteogenesis at the bone defect.

5 Conclusions

Novel 3D scaffolds made of nano non-stoichiometric apatite and poly(ε-caprolactone) bioactive composites were fabricated using a prototyping controlled process. The pore size, morphology, and interconnectivity were well controlled by the PCP technology. The prepared ns-AP/PCL composite scaffolds had a high porosity of 76%, with open and interconnected pores size ranging from 400 to 500 μm. Proliferation of MG_{63} cells was significantly higher on the composite scaffolds with porosity of 76% than those with porosity of 53%, demonstrating that the high porosity of composite scaffolds facilitated the cell growth and proliferation. The well-interconnected pore structure of the ns-AP/PCL composite scaffold encouraged bone cell ingrowth and distribution, with no negative effects on bone tissue formation. According to the radiographic and histological evaluations, the ns-AP/PCL composite scaffold implants exhibited high efficiency of bone regeneration. Our results suggest that the scaffold had good biocompatibility, biofunctionality, and enhanced osteogenesis.

Acknowledgements The authors would like to thank Ms. Fan Minghui from Institute of Chemistry and Materials Science, University of Science and Technology of China for her assistance in material preparation of this paper.

References

1. Motskin M, Wright DM, Muller K, Kyle N, Gard TG, Porter AE, et al. Hydroxyapatite nano and microparticles: correlation of particle properties with cytotoxicity and biostability. Biomaterials. 2009;30:3307–17.
2. Zou Q, Li YB, Zhang L, Zuo Y, Li JF, Li JD. Antibiotic delivery system using nano-hydroxyapatite/chitosan bone cement consisting of berberine. J Biomed Mater Res A. 2009;89:1108–17.
3. Dorozhkin SV. Calcium orthophosphate-based biocomposites and hybrid biomaterials. J Mater Sci. 2009;44:2343–87.
4. Balasundaram G, Webster TJ. An overview of nano-polymers for orthopedic applications. Macromol Biosci. 2007;7:635–42.
5. Best SM, Porter AE, Thian ES, Huang J. Bioceramics: past, present and for the future. J Eur Ceram Soc. 2008;7:1319–27.
6. Shor L, Guceri S, Wen XJ, Gandhi M, Sun W. Fabrication and cell-matrix interaction study on three-dimensional polycaprolactone/hydroxyapatite tissue scaffolds. Biomaterials. 2007;28:5291–7.

7. Rhee SH, Choi JY, Kim HM. Preparation of a bioactive and degradable poly(epsilon-caprolactone)/silica hybrid through a sol-gel method. Biomaterials. 2002;23:4915–21.
8. Baker SC, Rohman G, Southgate J, Cameron NR. The relationship between the mechanical properties and cell behaviour on PLGA and PCL scaffolds for bladder tissue engineering. Biomaterials. 2009;30:1321–8.
9. Rhee SH. Effect of molecular weight of poly(epsilon-caprolactone) on interpenetrating network structure, apatite-forming ability, and degradability of poly(epsilon-caprolactone)/silica nano-hybrid materials. Biomaterials. 2003;24:1721–7.
10. Yeo A, Rai B, Sju E, Cheong JJ, Teoh SH. The degradation profile of novel, bioresorbable PCL-TCP scaffolds: an in vitro and in vivo study. J Biomed Mater Res A. 2008;84:208–18.
11. Aizawa M, Ueno H, Itatani K, Okada I. Syntheses of calcium-deficient apatite fibres by a homogeneous precipitation method and their characterizations. J Eur Ceram Soc. 2006;4–5:501–7.
12. Sachlos E, Gotora D, Czernuszka JT. Collagen scaffolds reinforced with biomimetic composite nano-sized carbonate-substituted hydroxyapatite crystals and shaped by rapid prototyping to contain internal microchannels. Tissue Eng. 2006;9:2479–87.
13. Kannan S, Pina S, Ferreira JMF. Formation of strontium-stabilized β-tricalcium phosphate from calcium-deficient apatite. J Am Ceram Soc. 2006;89(10):3277–80.
14. Mobini S, Javadpour J, Hosseinalipour M, Ghazi-Khansari M, Khavandi A, Rezaie HR. Synthesis and characterisation of gelatin-nano hydroxyapatite composite scaffolds for bone tissue engineering. Adv Appl Ceram. 2008;107(1):4–8.
15. Huang YX, Ren J, Chen C, Ren TB, Zhou XY. Preparation and properties of poly(lactide-co-glycolide) (PLGA)/nano-hydroxyapatite (NHA) scaffolds by thermally induced phase separation and rabbit MSCs culture on scaffolds. J Biomater Appl. 2008; 22(5):409–32.
16. Jose MV, Thomas V, Johnson KT, Dean DR, Nyalro E. Aligned PLGA/HA nanofibrous nanocomposite scaffolds for bone tissue engineering. Acta Biomater. 2009;5(1):305–15.
17. Peltola SM, Melchels FPW, Grijpma DW, Kellomaki M. A review of rapid prototyping techniques for tissue engineering purposes. Ann Med. 2008;40:268–80.
18. Yousefi AM, Gauvin C, Sun L, DiRaddo RW, Fernandas J. Design and fabrication of 3D-plotted polymetric scaffolds in functional tissue engineering. Polym Eng Sci. 2007;47:608–18.
19. Cahill S, Lohfeld S, McHugh PE. Finite element predictions compared to experimental results for the effective modulus of bone tissue engineering scaffolds fabricated by selective laser sintering. J Mater Sci Mater Med. 2009;20:1255–62.
20. Ge ZG, Wang LS, Heng BC, Tian XF, Lu K, Fan VTW, et al. Proliferation and differentiation of human osteoblasts within 3D printed poly-lactic-co-glycolic acid scaffolds. J Biomater Appl. 2009;23:533–47.
21. Yuan H, Kurashina K, de Groot K, Zhang X. A preliminary study on osteoinduction of two kinds of calcium phosphate ceramics. Biomaterials. 1999;20:1799–806.
22. Nejati E, Mirzadeh H, Zandi M. Synthesis and characterization of nano-hydroxyapatite rods/poly(L-lactide acid) composite scaffolds for bone tissue engineering. Composites A. 2008;39(10):1589–96.
23. Zhang PB, Hong ZK, Yu T, Chen XS, Jing XB. In vivo mineralization and osteogenesis of nanocomposite scaffold of poly (lactide-co-glycolide) and hydroxyapatite surface-grafted with poly(L-lactide). Biomaterials. 2009;30:58–70.
24. Hong Z, Zhang P, He C, Qiu X, Liu A, Chen L. Nano-composite of poly(L-lactide) and surface grafted hydroxyapatite: mechanical properties and biocompatibility. Biomaterials. 2005;32:6296–304.
25. Zhu X, Eibl O, Scheideler L, Geis-Gerstorfer Jurgen J. Characterization of nano hydroxyapatite/collagen surfaces and cellular behaviors. Biomed Mater Res A. 2006;79(1):114–127.
26. Zhou DS, Zhao KB, Li Y, Cui FZ, Lee IS. Repair of segmental defecits with nano-hydroxyapatite/collagen/PLA composite combined with mesenchymal stem cells. J Bioact Compat Polym. 2006;5:373.
27. Khang D, Kim SY, Liu-Snyder P, Palmore GTR, Durbin SM, Webster TJ. Enhanced fibronectin adsorption on carbon nanotube/poly(carbonate) urethane: independent role of surface nanoroughness and associated surface energy. Biomaterials. 2007; 28(32):4756–68.
28. Zhang LJ, Ramsaywack S, Fenniri H, Webster TJ. Enhanced osteoblast adhesion on self-assembled nanostructured hydrogel scaffolds. Tissue Eng A. 2008;14:1353–64.